Available online at www.sciencedirect.com
ScienceDirect
Mathematics and Computers in Simulation 74 (2007) 361–369
MATHEMATICS AND COMPUTERS IN SIMULATION
www.elsevier.com/locate/matcom

Soliton trains and vortex streets as a form of Cerenkov radiation in trapped Bose–Einstein condensates

R. Carretero-González[a], P.G. Kevrekidis[b], D.J. Frantzeskakis[c], B.A. Malomed[d,*], S. Nandi[b], A.R. Bishop[e]

[a] *Nonlinear Dynamical Systems Group,*[1] *Department of Mathematics and Statistics, San Diego State University, San Diego, CA 92182-7720, USA*
[b] *Department of Mathematics and Statistics, University of Massachusetts, Amherst, MA 01003-4515, USA*
[c] *Department of Physics, University of Athens, Panepistimiopolis, Zografos, Athens 15784, Greece*
[d] *Department of Interdisciplinary Studies, Faculty of Engineering, Tel Aviv University, Tel Aviv 69978, Israel*
[e] *Center for Nonlinear Studies and Theoretical Division, Los Alamos National Laboratory, Los Alamos, NM 87545, USA*

Available online 6 December 2006

Abstract

We numerically study the nucleation of gray solitons and vortex–antivortex pairs created by a moving impurity in, respectively, 1D and 2D Bose–Einstein condensates (BECs) confined by a parabolic potential. The simulations emulate the motion of a localized laser-beam spot through the trapped condensate. Our results for the 1D case indicate that, due to the inhomogeneity of the BEC density, the critical speed for nucleation, as a function of the condensate density displays two distinct dependences. In particular, the square root of the critical density for nucleation as a function of speed displays two different linear regimes corresponding to small and large velocities. Effectively, the emission of gray solitons and vortex–antivortex pairs occurs for any velocity of the impurity, as any given velocity will be supercritical in a region with a sufficiently small density. At longer times, the first nucleation is followed by generation of an array of solitons in 1D ("soliton train") or vortex pairs in 2D ("vortex street") by the moving object.

Keywords: Bose–Einstein condensation; Solitons; Vortices; Nucleation; Matter waves

1. Introduction

Since the discovery of superfluidity in helium in the late 1930s [1], there has been a large amount of interest in the investigation of the breakdown of superfluidity and the concomitant generation of elementary excitations in quantum gases. In particular, after the realization of Bose–Einstein condensates (BECs) in dilute alkali atom gases [2], much experimental and theoretical effort has been devoted to the understanding of important relevant concepts, such as the critical velocity introduced by Landau, sound waves and the speed of sound, vortices and solitons, and so on (see, e.g. reviews [6]).

From the theoretical view point, the nonlinear Schrödinger (NLS) equation [*alias* Gross–Pitaevskii (GP) equation in the BEC context] has attracted attention as a model of superflow, i.e. flow with zero viscosity, see, e.g. [8]. This

* Corresponding author. Fax: +972 3 640 6399.
E-mail address: malomed@post.tau.ac.il (B.A. Malomed).
[1] http://nlds.sdsu.edu.

0378-4754/$32.00
doi:10.1016/j.matcom.2006.10.033

model has been used to study the flow of a BEC around an obstacle, leading to vortex emission and formation of bow waves [20,10,16]. The motion of a heavy impurity through a condensate has also been analyzed by means of a perturbative approach [3]. In lower-dimensional settings, the formation of dark solitons induced by the motion of an obstacle in static BECs [9,17], or in the presence of a static localized impurity in oscillating BECs [19], has also been considered. Additionally, in the case of large obstacles, it has recently been shown that for a supersonic flow of a BEC, the Cerenkov cone transforms into a spatial shock wave consisting of a chain of dark solitons [7]. Cerenkov radiation is referred to as emission of shock waves by a body propagating with a speed larger than the speed of sound of the medium [5]. Furthermore, in the same (quasi-1D) setting, the breakdown of superfluidity has also been considered [15]. Apart from the above theoretical studies, one should also mention the detailed experiments of Refs. [18,14], demonstrating the onset of dissipation induced by the motion of an impurity (in the form of a blue-detuned laser beam) through the condensate for velocities only above a critical velocity, and the experiments of Ref. [21] where slow light pulses were shown to generate trains of dark solitons, via the creation of quantum shock waves. Finally, it should be noted that the appearance of similar effects (e.g. the backward-propagating Cerenkov radiation) in optical media, such as photonic crystals [12], illustrates the importance of a better understanding of the relevant phenomenology, not only qualitatively, but also quantitatively.

In this work we focus on a detailed numerical study of an *inhomogeneous* BEC, confined in one- or two-dimensional traps. While most of the above-mentioned studies focused on homogeneous superfluids, there are some works (see, e.g. [10]), which were concerned with the case of a condensate with an inhomogeneous density distribution. Our main findings, which also highlight differences from the previous works, include the following:

- In the trapped BEC, emission of coherently structured radiation always occurs, i.e. for any speed of the body moving across the condensate. This is due to the fact that any given velocity turns out to be supersonic in a part of the system where the density is small enough.
- In the 1D case, the critical density η_c for the nucleation of gray solitons features two different dependences on the speed of the traveling impurity. Specifically, we find that $\eta_c^{1/2}$ obeys two linear dependences for small and large velocities, respectively. For small velocities, the dependence is well approximated by the perturbative approach developed in Ref. [9] for homogeneous NLS flows. The second regime, observed at large velocities, can be attributed to the nonadiabatic character of the dynamics driven by the impurity moving through the inhomogeneous medium. This regime is not straightforwardly amenable to an analytical treatment.
- In the 1D and 2D cases, the coherently structured radiation assumes the form of gray solitons and vortex dipoles, respectively. Longer evolution results in the formation of such structures arranged in continuously expanding trains.

Among these points, the first (and partially the third, as concerns vortex dipoles) was also reported in Ref. [10]. The second point offers a rather different view on the critical condition for generation of radiation by a small moving body, which is one of the key contributions of the present work. Furthermore, as regards both the second and the third points, detailed 1D numerical experiments presented here (the 1D case was not examined in Ref. [10]) offer new insights on the generation of "coherent-structure radiation" and identifying the threshold for this phenomenon.

Our presentation is structured as follows. In Sections 2 and 3, we report numerical results for the 1D and 2D cases, respectively. In Section 4, we summarize the findings and present conclusions, also highlighting issues for future studies.

2. The one-dimensional model

We start with the normalized GP equation, which governs the evolution of the single-atom BEC wave function in the mean-field approximation [6]:

$$i\partial_t u = -\partial_x^2 u + |u|^2 u + [V_1(x) + V_2(x,t)]u \tag{1}$$

where

$$V_1(x) = \frac{1}{2}\Omega^2 x^2 \tag{2}$$

represents the external harmonic trapping potential with strength Ω, and $V_2(x)$ accounts for a body (or an impurity) moving across the condensate. This potential term is approximated by the expression:

$$V_2(x,t) = V_0 \exp\left(-\frac{(x-vt)^2}{\epsilon^2}\right) \tag{3}$$

where the parameters V_0, ϵ and $v > 0$ describe the amplitude, width and velocity of the impurity, respectively. Actually, if this moving obstacle emulates a laser-beam spot, the Gaussian shape adopted in Eq. (3) is the most natural one. Note that the trap strength Ω, along with the chemical potential μ, define the spatial size of the condensate, i.e. the Thomas–Fermi radius given by $R_{\mathrm{TF}} = \sqrt{2\mu}/\Omega$. This is the so-called Thomas–Fermi approximation [6], which provides a fairly good description of the condensate density (in the absence of the moving body):

$$\eta_{\mathrm{TF}}(x) \equiv |u_{\mathrm{TF}}(x)|^2 \approx \begin{cases} \mu - V_1(x), & \text{if } \mu - V_1(x) > 0 \\ 0, & \text{if } \mu - V_1(x) \leq 0 \end{cases} \tag{4}$$

Without loss of generality, the normalization $\mu = 1$ is adopted throughout this work.

In the simulations presented below, we choose several values for the impurity parameters in intervals $V_0 \in [0.25, 1]$ and $\epsilon^2 \in [0.09, 1.5]$. Our simulations were typically performed in a spatial discretization of 2000 grid points using a second order spatial finite difference scheme with a Runge–Kutta fixed-time integrator. We perform the simulations in the presence of the trapping potential, $V_1(x)$, to observe effects of spatial inhomogeneity on the generation of radiation. The simulations are started by an initial condition given by the steady state of the condensate when the impurity is at rest ($v = 0$) at the center of the external harmonic trap. This steady state is found numerically by means of fixed point iterations (Newton's method) until the solution converges to numerical accuracy. A typical scenario of an impurity traversing the condensate is depicted in Fig. 1 where two examples for different impurity velocities are presented. As it is clear from the figure, the faster impurity (middle row panels) is able to emit radiation, in the form of dark solitons (as evidenced by the phase dislocations depicted in the right panels), earlier (i.e. already for higher densities). To be more precise, the emitted dark solitons are gray ones, since they move (after completely detaching from the impurity, they slide to the left).

To gain a deeper insight into the generation of dark solitons by the moving body and to connect it to the Cerenkov's radiation, emitted by a particle moving in a medium with a supersonic velocity, we perform the following sequence of numerical experiments. For various speeds, an instant was identified when the first emitted soliton detaches from the body. The identification of this time (we define it as an instant when the distance between the body and the soliton becomes larger than a certain fixed length) is somewhat arbitrary. However, (a) the sharpness of the separation and the speed at which it happens (due to the much larger speed of the body than that of the emitted soliton) and (b) the low impurity velocities, $v < 1$, that we use (so that small discrepancies on the detection of the nucleation time do not have any significant impact on the determination on the nucleation density) allows us to implement this procedure in a fairly precise way. We define the separation time as that when the relative difference in the position between the two entities becomes larger than 10^{-3}. By identifying the position of the waves at that time, we can then measure the density at the separation point in space, and adopt it as a critical density η_{c} for the separation of the gray soliton.

Typical results of this computation for various values of the parameters V_0 and ϵ as a function of the impurity speed v are presented in Fig. 2. Error bars in the figure represent the values for the density corresponding to the position of the impurity with a tolerance determined by the finite width of the impurity, the error bar being larger for a wider impurity and/or steeper density profile. The examples presented in the figure make it clear that there exist two distinct linear dependences of $\eta_{\mathrm{c}}^{1/2}$ on v (open and filled circles). The first regime, corresponding to the linear dependence at small v (open circles), is essentially adiabatic, and it can therefore be well approximated by the emission of gray solitons in a locally homogeneous NLS flow past an obstacle [9]. The respective critical velocity for the emission can be approximated, using perturbation techniques, for weak potentials by the expression:

$$v_{\mathrm{c}} = \sqrt{2} - \frac{3}{2\sqrt{2}}\left[\int_{-\infty}^{\infty} V_2(x)\,\mathrm{d}x\right]^{2/3} \tag{5}$$

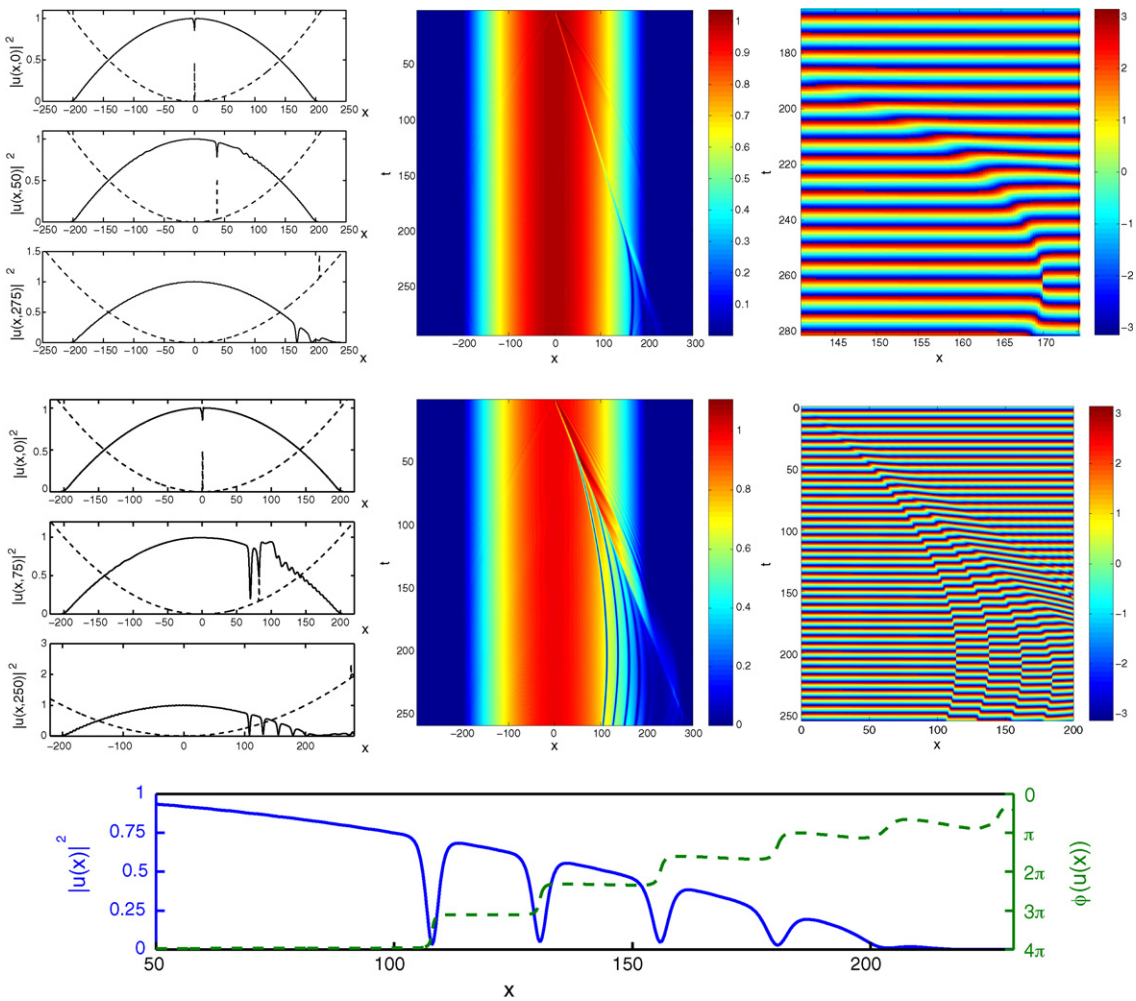

Fig. 1. Two cases of the motion of the body (top two rows), characterized by an amplitude $V_0 = 0.5$ and width $\epsilon^2 = 0.09$, through the inhomogeneous (trapped) condensate with a TF radius $R_{\mathrm{TF}} = 200$. Top and middle rows correspond, respectively, to velocities $v = 0.75$ and 1.1. In each case, the left panels show the spatial profiles of the BEC density (squared absolute value of the wave function) for three different times (the potential is shown by the dashed line). The middle panel shows contour plots of the density and its spatio-temporal evolution. The right panel displays the spatiotemporal evolution of the phase, revealing the presence of phase dislocations (and thus demonstrating the formation of gray solitons). Bottom panel: detail of the density distribution (solid line) after nucleation ($t = 250$) together with the phase of the solution $\phi(u(x))$ (dashed line) for the $v = 1.1$ case. The magnitude of each phase dislocation determines the velocity of the gray soliton: a phase dislocation of π corresponds to a quiescent dark soliton while in the limit of infinitesimal phase dislocation the velocity tends to the speed of sound at the particular location of the dislocation.

for the homogeneous density $\eta \equiv 1$ (see Eq. (32) in Ref. [9]). In our context, this translates into the following approximation for the critical density η_c as a function of the impurity speed v:

$$\eta_c^{1/2} = \alpha v = \left[\sqrt{2} - \frac{3\pi^{1/3}}{2\sqrt{2}}(\epsilon V_0)^{2/3}\right]^{-1} v \tag{6}$$

As seen in Fig. 2, the solid line corresponding to approximation (6) captures the behavior at small velocities fairly well. It would be in principle possible to consider a smooth approximation to the critical nucleation density versus speed; however, as there are two clear linear regimes (for small speeds the critical nucleation density behaves like in Eq. (6) and for larger speeds there seems to be a consistent saturation of the slope towards $a = 1$) we opt to use a piece-wise linear description. Another point worth elaborating is the fact that since we have fixed, without loss of generality, the chemical potential to $\mu = 1$, for velocities larger than $v = 1$ the impurity is always supersonic and thus the critical density saturates. Therefore, all our results are presented for $v < 1$.

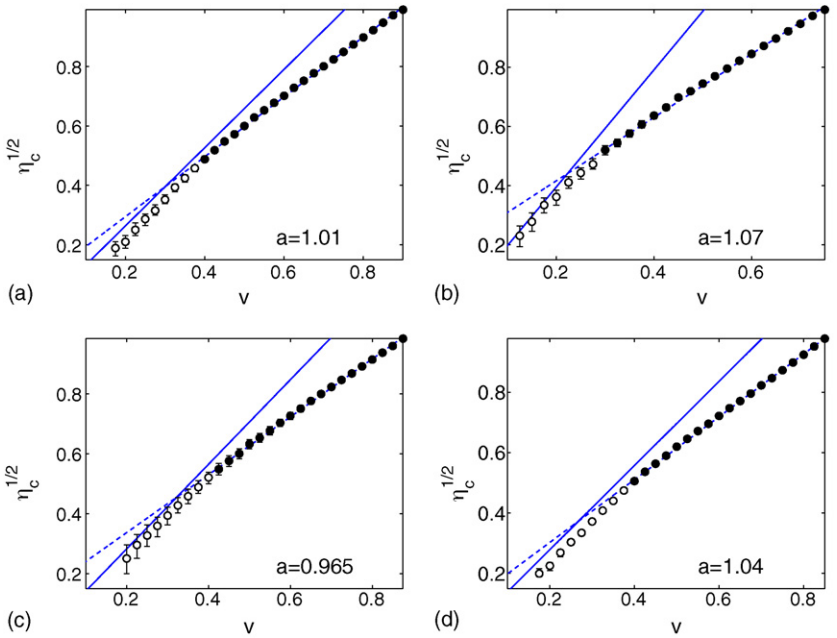

Fig. 2. Critical density for the nucleation of a gray soliton, by a moving body, inside a condensate trapped by the external harmonic potential (2). The solid line represents the approximation given in Eq. (6) and the dashed line represents the linear fit $\eta_c^{1/2} = av + b$ for the linear regime depicted by the filled dots. The slope a for this fit is indicated in each panel. The error bars correspond to the densities measured one impurity width before and after the impurity's center. The condensate has a radius $R_{TF} = 200$ and the body's parameter values are: (a) $\epsilon^2 = 0.3$, $V_0 = 0.5$; (b) $\epsilon^2 = 0.8$, $V_0 = 0.5$; (c) $\epsilon^2 = 1.5$, $V_0 = 0.25$; (d) $\epsilon^2 = 0.09$, $V_0 = 1$.

For larger velocities the above approximation is no longer valid, and the nucleation of dark solitons tends to occur later than predicted by Eq. (6). This fact is not difficult to understand qualitatively if we take into account that the nucleation of the gray soliton does not happen instantaneously. Therefore, even if the moving impurity has reached a region with the critical density, it takes some time for the gray soliton to be nucleated, and thus, when it finally emerges, the density is actually lower. An interesting feature, evident in Fig. 2, is that η_c follows a practically linear relationship for large velocities too, albeit with a different slope. Data corroborating the nearly linear regime at high velocities are shown by filled circles in Fig. 2, together with the respective linear fit (dashed line). Even more surprising is the fact that the slope in this regime (parameter a in each panel in Fig. 2) is very close to 1. The latter observation raises an interesting question concerning the systematic difference (by a factor of $\approx \sqrt{2}$) of the slope of the speed versus square root of density dependence, in comparison to the corresponding local speed of sound [the sound velocity $\sqrt{2}$ is represented by the first term in the square brackets in Eq. (6)].

In order to corroborate these results and check their generality, we conducted a similar numerical experiment with the condensate trapped in the piecewise linear potential:

$$V_1(x) = \Omega|x| \tag{7}$$

The motivation for this choice is to check whether a linear potential is able to reproduce the same effects found for the quadratic potential (2). Note that in this case the spatial size of the condensate is determined by the TF radius which is now given by $R_{TF} = \mu/\Omega$. Without loss of generality, we again fix $\mu = 1$. The critical nucleation density for different values of impurity parameters is depicted, as a function of the impurity's velocity, for the present case in Fig. 3. As in the case of the parabolic external trap (2), the results reveal two well-pronounced linear regimes: for small velocities, there is a good match to approximation (6), and for larger velocities a good approximation is $\eta_c^{1/2} = av + b$, with the slope a again very close to 1 for different choices of the parameters, b being a (typically, small) offset parameter of the fit.

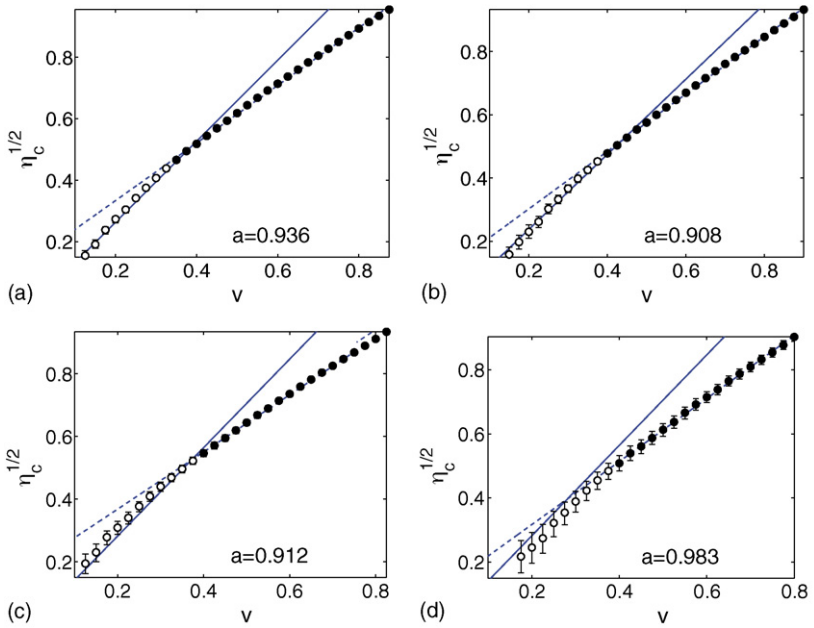

Fig. 3. Critical density for the nucleation of a gray soliton as in Fig. 2 but with the piecewise linear potential (7). The parameter values are: (a) $\epsilon^2 = 0.3$, $V_0 = 0.5$, $R_{TF} = 200$; (b) $\epsilon^2 = 0.8$, $V_0 = 0.25$, $R_{TF} = 200$; (c) $\epsilon^2 = 1.5$, $V_0 = 0.25$, $R_{TF} = 200$; (d) $\epsilon^2 = 1.5$, $V_0 = 0.25$, $R_{TF} = 100$.

Another interesting phenomenon can also be observed in Fig. 1. The generation of solitons occurs so as to decrease the local propagation speed (due to the velocity field induced by the generated wave). However, as the body moves farther away from the solitary wave which it has created, the velocity field of the soliton is no longer sufficient to keep the velocity below its critical value, hence the body again becomes supercritical, starting to generate another solitary wave. In this way, a train of solitons is produced. In Fig. 1, four such waves are clearly discernible in the bottom panel. Fig. 4 shows (in the same context) the distance between the generated waves (which appears to be approximately constant) as a function of the body's speed. As expected, the faster the source, the smaller the interval of time during which its speed may be made subcritical by generation of a soliton and hence the shorter the distance until a new soliton is generated.

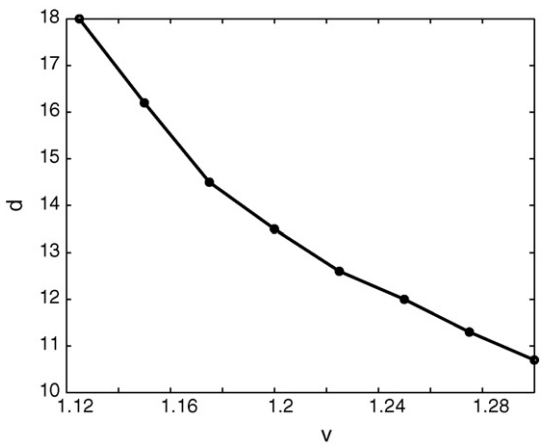

Fig. 4. Distance between solitons (i.e. phase dislocations) in the generated soliton train as a function of the source's speed. Parameter values are $R_{TF} = 200$, $V_0 = 0.5$ and $\epsilon^2 = 0.09$.

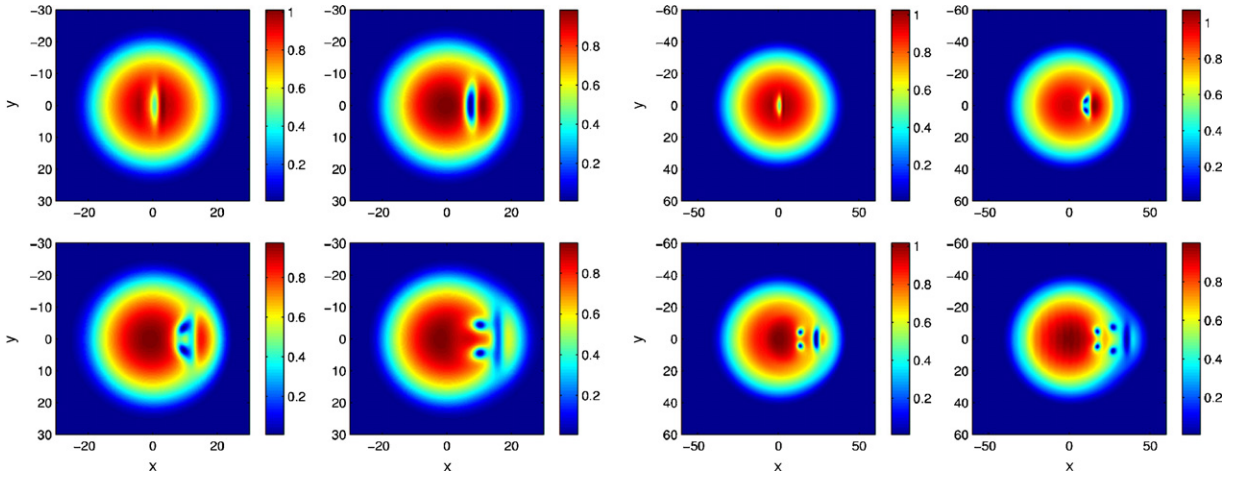

Fig. 5. The left panels show the case of the motion of the immersed body in two dimensions with velocity $v = 0.8$. The density contour plots are shown at times $t = 1$ (top left), $t = 10$ (top right), $t = 15$ (bottom left), and $t = 20$ (bottom right). The TF radius is $R_{\mathrm{TF}} = 23.57$ (or $\Omega = 0.06$). The right set of panels corresponds to the case with $v = 0.8$, but now for $R_{\mathrm{TF}} = 40.40$ (or $\Omega = 0.035$) [for the same transverse width parameter, $\beta = 0.03$, see Eq. (8)]. The snapshots are shown at times, respectively, $t = 0$ (top left), $t = 15$ (top right, when the first vortex pair nucleates), $t = 30$ (bottom left, the second pair starts nucleating) and $t = 45$ (bottom right).

3. The two-dimensional model

Similar results can be obtained in the 2D setting, i.e. for a disk-shaped BEC, described by the 2D version of the GP Eq. (1), with the operator ∂_x^2 being replaced by the Laplacian $\nabla^2 = \partial_x^2 + \partial_y^2$. In this case, the 2D trapping potential, together with the moving source, is defined as follows:

$$V(x,t) = \frac{1}{2}\Omega^2\left(x^2 + y^2\right) + V_0 \exp\left(-\frac{(x - vt)^2 + \beta y^2}{\epsilon^2}\right) \tag{8}$$

For this setting, we only present "proof-of-principle" simulations, rather than a detailed quantitative analysis. In the 2D case, the impurity should be sufficiently anisotropic (or isotropic but sufficiently wide), so as to permit the generation of the relevant 2D coherent structures, namely vortex pairs. In fact, we have observed that, if the external trap is sufficiently strong (e.g. for $\Omega > 0.2$ or $R_{\mathrm{TF}} < 7$), then there is not enough room for the vortex dipole to nucleate and, hence, independently of the potential anisotropy of the impurity, vortex pairs will not be emitted. However, for sufficiently weak external traps (see also a similar discussion in Ref. [11]) such dipoles will be generated.

We have used $\epsilon = V_0 = 1$ and $\beta = 0.03$ as typical parameters for the results shown in Fig. 5; for the condensate, we have assumed that $R_{\mathrm{TF}} = 23.57$ and 40.40 (or $\Omega = 0.06$ and 0.035) for the left and right quartet of panels, respectively.

For very large velocities v, when the motion of the body is definitely supercritical, we observed that the vortex pairs nucleate very quickly (data not shown). On the other hand, if the initial speed is initially slightly subcritical, then, as in the 1D case, the impurity moves until it arrives at a critical point, where $v \approx \eta^{1/2}$. After passing this point, a vortex pair is created. This has been tested similarly to the 1D case. It has been found, e.g. that for $v = 0.8$, the pair is generated when the density is ≈ 0.830, while for $v = 0.9$, it is generated when the density is ≈ 0.919, in close agreement with the proposed criterion. The case with $v = 0.8$ is shown in the left panels of Fig. 5. A general effect, similar to that described above for the 1D situation, is observed: after the already generated vortex dipole flow becomes insufficient to keep the body's speed below the threshold value, another vortex pair is created. In this way, a "vortex street" forms, consisting of the generated vortex dipoles (shown in the right part of Fig. 5).

4. Conclusions and outlook

In this work, we have considered the generation of coherent matter-wave radiation by a small body moving through a Bose–Einstein condensate (BEC). We have performed numerical experiments for 1D and 2D trapped BECs. Our results have demonstrated the absence of a cutoff speed in the inhomogeneous condensate below which no radiation

is emitted. When the body moves in a region where the density exceeds the critical value, the motion is subcritical, and radiation is not emitted. When the local density falls below the critical level, η_c, the speed becomes supercritical, and the generation of radiation starts, in the form of gray solitons in the 1D case, and vortex–antivortex pairs in the 2D setting. Specifically, for the 1D case we have shown that the critical density η_c, considered as a function of the impurity speed v, can display two distinct dependences. The first regime occurs at small v, when the local value of the density can be used to predict the critical velocity as in the uniform medium, with a small adiabatic correction. This approximation leads to $\eta_c^{1/2}$ being proportional to v, with the proportionality constant well-approximated by the perturbative result of Ref. [9]. The second regime occurs at larger values of v, where the adiabatic approximation obviously fails. In this case, a linear relationship was found, in the form $\eta_c = av + b$ with $a \approx 1$ and $b > 0$. Explanation of the seemingly parameter-independent value of the slope (a) poses a challenge for subsequent work in this field.

Another particular issue that has emerged in this study and which deserves further investigation is the generation of regularly spaced soliton trains and vortex streets by the supersonic body. It would be particularly interesting to examine the velocity field near the small body, in the absence and in the presence of a wave. Given such a velocity field of the previously created gray soliton or vortex dipole [13], it would be interesting to find a "quantization condition" that could explain the spacing in the observed train of coherent wave excitations.

A problem of a different kind in the 2D geometry may be generation of (possibly coherently structured) radiation by a small impurity which performs spiral or circular motion, i.e. moves through the region with a constant density. Also interesting could be various regimes of the generation of radiation in the 2D case when the background state itself is a vortex, rather than a quiescent TF configuration.

Clearly, it would also be of interest to extend these considerations to a three-dimensional setting, and observe the corresponding excitations (such as, e.g. vortex rings [4]) that would be produced in that case. Such studies are currently in progress and will be reported elsewhere.

Acknowledgements

We would like to acknowledge two anonymous reviewers for their valuable comments and suggestions. PGK gratefully acknowledges support from NSF-DMS-0204585, NSF-CAREER. RCG and PGK also acknowledge support from NSF-DMS-0505663. Work at Los Alamos is supported by the US DoE.

References

[1] J.F. Allen, A.D. Misen, Nature (London) 141 (1938) 75;
P.L. Kapitza, Nature (London) 141 (1938) 74.
[2] M.H. Anderson, et al., Science 269 (1995) 198;
K.B. Davis, et al., Phys. Rev. Lett. 75 (1995) 3969;
C.C. Bradley, et al., Phys. Rev. Lett. 75 (1995) 1687.
[3] G.E. Astracharchik, L.P. Pitaevskii, Phys. Rev. A 70 (2004) 013608.
[4] N.G. Berloff, Phys. Lett. A 277 (2000) 240;
N.G. Berloff, Phys. Rev. B 65 (2002) 174518;
S. Komineas, N. Papanicolaou, Phys. Rev. Lett. 89 (2002) 070402;
N.S. Ginsberg, J. Brand, L.V. Hau, Phys. Rev. Lett. 94 (2005) 040403.
[5] P.A. Čerenkov, Nobel Lecture, December 11, 1958. Radiation of Particles Moving at a Velocity Exceeding That of Light, and Some of the Possibilities for Their Use in Experimental Physics. Nobel Lectures, Physics 1942–1962, Elsevier Publishing Company, Amsterdam, 1964.
[6] F. Dalfovo, S. Giorgini, L.P. Pitaevskii, S. Stringari, Rev. Mod. Phys. 71 (1999) 463–512;
P.G. Kevrekidis, D.J. Frantzeskakis, Mod. Phys. Lett. B 18 (2004) 173;
V.A. Brazhnyi, V.V. Konotop, Mod. Phys. Lett. B 18 (2004) 627;
P.G. Kevrekidis, R. Carretero-González, D.J. Frantzeskakis, I.G. Kevrekidis, Mod. Phys. Lett. B 18 (2005) 1481.
[7] G.A. El, A.M. Kamchatnov, Phys. Lett. A 350 (2006) 192;
G.A. El, A. Gammal, A.M. Kamchatnov, Phys. Rev. Lett. 97 (2006) 180405.
[8] T. Frisch, Y. Pomeau, S. Rica, Phys. Rev. Lett. 69 (1992) 1644;
C. Josserand, Y. Pomeau, S. Rica, Phys. Rev. Lett. 75 (1995) 3150.
[9] V. Hakim, Phys. Rev. E 55 (1997) 2835.
[10] B. Jackson, J.F. McCann, C.S. Adams, Phys. Rev. Lett. 80 (1998) 3903;
B. Jackson, J.F. McCann, C.S. Adams, Phys. Rev. A 61 (2000) 051603(R).
[11] P.G. Kevrekidis, G. Theocharis, D.J. Frantzeskakis, A. Trombettoni, Phys. Rev. A 70 (2004) 023602.

[12] C. Luo, M. Ibanescu, S.G. Johnson, J.D. Joannopoulos, Science 299 (2003) 368.
[13] P.K. Newton, Discrete Contin. Dyn. Syst. B 2005 (Suppl.) (2005) 692.
[14] R. Onofrio, C. Raman, J.M. Vogels, J.R. Abo-Shaeer, A.P. Chikkatur, W. Ketterle, Phys. Rev. Lett. 85 (2000) 2228.
[15] N. Pavloff, Phys. Rev. A 66 (2004) 013610.
[16] C.-T. Pham, C. Nore, M.-E. Brachet, Physica D 210 (2005) 203.
[17] A. Radouani, Phys. Rev. A 70 (2004) 013602.
[18] C. Raman, M. Köhl, D.S. Durfee, C.E. Kuklewicz, Z. Hadzibabic, W. Ketterle, Phys. Rev. Lett. 83 (1999) 2502.
[19] G. Theocharis, P.G. Kevrekidis, H.E. Nistazakis, D.J. Frantzeskakis, A.R. Bishop, Phys. Lett. A 337 (2005) 441.
[20] T. Winiecki, J.F. McCann, C.S. Adams, Phys. Rev. Lett. 82 (1999) 5186;
B. Jackson, J.F. McCann, C.S. Adams, Phys. Rev. A 61 (2000) 013604.
[21] Z. Dutton, M. Budde, C. Slowe, L.V. Hau, Science 293 (2001) 663, and Science Express, June 28, 2001.